VIII International Conference on Fracture Mechanics of Concrete and Concrete Structures
FraMCoS-8
J.G.M. Van Mier, G. Ruiz, C. Andrade, R.C. Yu and X.X. Zhang (Eds)

# MODELLING CRACK INITIATION AND PROPAGATION IN MASONRY USING THE PARTITION OF UNITY METHOD

**B. VANDOREN*, K. DE PROFT*, A. SIMONE† AND L. J. SLUYS†**

*Hasselt University
Physics Capacity Group
Agoralaan Gebouw D, 3590 Diepenbeek, Belgium
e-mail: bram.vandoren@uhasselt.be

†Delft University of Technology
Faculty of Civil Engineering and Geosciences
P.O. Box 5048, 2600 GA Delft, The Netherlands

**Key words:** Masonry, Partition of Unity, Mesoscopic Model

**Abstract.** A mesoscopic masonry model is presented using the partition of unity finite element method. Joints are only explicitly introduced when a critical stress state is exceeded, resulting in a computationally more efficient procedure when compared to models in which all joints are a priori active. The performance of the presented model is demonstrated by several numerical examples.

## 1 INTRODUCTION

Although an ancient building technique, masonry is still widely used in modern structures due to its relatively simple way of constructing. The failure modelling of these structures remains, however, a great challenge due to their composite nature. Two major modelling scales exist: macroscopic and mesoscopic. The former approach homogenises bricks and joints to one orthotropic material [1, 2] whereas in mescoscale models bricks and joints are modelled as separate entities, resulting in a more detailed crack pattern at the expense of more degrees of freedom and, consequently, yields a higher computational cost [3–7]. Recently, multiscale models have been developed and optimised to bridge the two modelling scales [8–11].

The masonry model presented in this contribution is a mesoscopic model in which the mortar joints are incorporated as potential strong discontinuities using the partition of unity method [12] as discussed in Section 2. The enhanced degrees of freedom, stemming from this technique, govern the nonlinear joint behaviour [13]. In contrast to classical mesoscopic masonry models, the joints are not active at the beginning of the calculation, resulting in less degrees of freedom. If a critical stress state is exceeded, the joint is activated and the corresponding enhanced degrees of freedom are added to the global system of equations. The employed material model, a shifted damage law based on a degenerated Drucker-Prager criterion, is presented in Section 3. This section will also address a modified equilibrium path-following procedure used in this study. In Section 4, three numerical examples are given in order to show the performance of the new masonry model.

## 2 MESOSCOPIC MODELLING OF MASONRY USING THE PARTITION OF UNITY METHOD

### 2.1 Kinematic description of the masonry model

In the presented two-dimensional mesoscopic masonry model, a partition of unity method is adopted in which the behaviour of each brick is governed by a designated set of enhanced degrees of freedom [13, 14]. Consequently, the displacement field can be decomposed according to

$$\mathbf{u} = \hat{\mathbf{u}} + \sum_{i=1}^{N_{\mathcal{B}}} \mathcal{H}_i \tilde{\mathbf{u}}_i \tag{1}$$

where $N_{\mathcal{B}}$ denotes the total number of bricks within the masonry wall, $\hat{\mathbf{u}}$ is the regular displacement field, $\tilde{\mathbf{u}}_i$ and $\mathcal{H}_i$ are the enhanced displacement field and enrichment function associated with brick $\mathcal{B}_i$, respectively. $\mathcal{H}_i = 1$ inside $\mathcal{B}_i$. A graphical representation of the assignment of the degrees of freedom is given in Figure 1. In order to avoid linear dependency of the enrichment functions, the total number of extra sets at each node should be reduced by one if the node contains more than one extra set of degrees of freedom as shown by Simone *et al.* [14]. This is illustrated in the lower part of the figure (Figure 1 (b)).

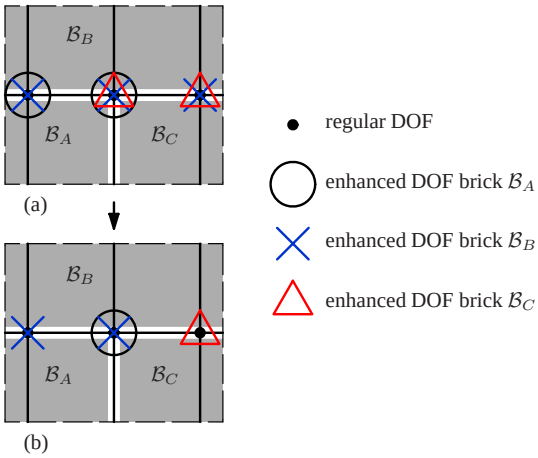


**Figure 1**: Assignment of the degrees of freedom (DOF) for a patch of masonry elements.

### 2.2 Activation of the enhanced degrees of freedom

The partition of unity framework allows a straightforward introduction of discontinuities, i.e. joints, without the need of a high dummy stiffness to mimic the pre-discontinuity phase. Enhanced degrees of freedom, representing the discontinuities, are simply added to the system when necessary. In short, the algorithm in this work is structured as follows: at the end of each load step (thus in a converged state), the stresses are evaluated at the joint positions through an interpolation of the stresses in the bulk material. If a critical stress state, governed by the material model presented in Section 3, is exceeded, all nodes on the critical joint are enhanced, i.e. extra degrees of freedom are added to the global system of equations. However, in the case that only two joints are active at the junction of three joints (joint BC and joint AC in Figure 2), additional constraints are necessary in order to prevent undesired joint opening of the inactive (subcritical) joint (joint AB in Figure 2). In the example of Figure 2, the constraint $\tilde{\mathbf{u}}_A - \tilde{\mathbf{u}}_B = 0$ is added to the system of equations.

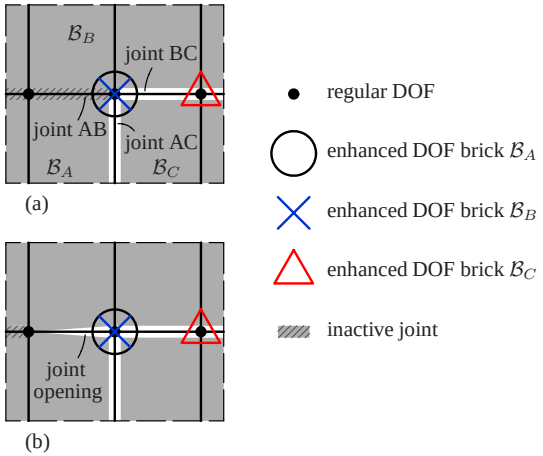


**Figure 2**: The need of additional constraints in case of an inactive joint (joint AB) at a triple junction of joints. (a) nomenclature; (b) undesired joint opening of the subcritical joint.

## 3 NONLINEAR MODELLING

### 3.1 Material model

In the developed masonry model, the brick behaviour remains linear elastic throughout the computation. However, since the mortar joints are inactive at the start of the simulation, the virgin material should also include the elastic behaviour of the mortar joints. Ideally, an anisotropic material model could be used, obtained from the homogenisation of the elastic mortar and brick behaviour. In this work a simpler approach is followed, similar to [3], in which the stiffness of the bulk material is adjusted in order to reproduce the experimental elastic response of the masonry structure. The adjusted Young's modulus $E_b'$ of the bricks then reads

$$E_b' = \alpha E_b \, . \tag{2}$$

The nonlinear joint behaviour is governed by a shifted damage law of the form

$$\mathbf{t}_d = (1-\omega)\, \mathbf{T}_d [\![\mathbf{v}]\!] \tag{3}$$

in which $\mathbf{t}_d$ is the traction at the joint, $\mathbf{T}_d = diag(k_n, k_t)$ is the joint stiffness matrix and $[\![\mathbf{v}]\!]$ represents the translated displacement jump at the mortar joint [15]

$$[\![\mathbf{v}]\!] = [\![\mathbf{u}]\!] + [\![\mathbf{u}]\!]_0 \, . \tag{4}$$

Figure 3 represents the shifted origin $[\![\mathbf{u}]\!]_0$, which is calculated from the bulk stress at the moment of joint activation.

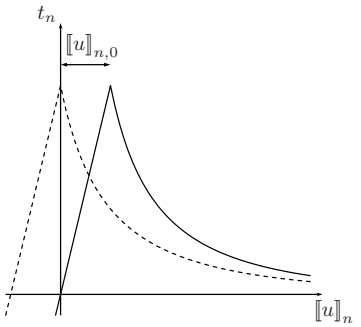


**Figure 3**: Pure mode I representation of the shifted damage law (dashed line).

The scalar damage variable $\omega$ in (3) is obtained from

$$\omega = \begin{cases} 0 & \text{if} \quad \kappa < \kappa_0 \\ 1 - \frac{\kappa_0}{\kappa} \exp\left[-\frac{\kappa-\kappa_0}{\beta}\right] & \text{if} \quad \kappa \geq \kappa_0 \end{cases} \tag{5}$$

where $\beta = \frac{h G_{f_I}}{f_t} - \frac{1}{2}\kappa_0$ in which $h$ denotes the joint thickness, $G_{f_I}$ is the mode-I fracture energy, $f_t$ is the uniaxial tensile strength of the mortar joints and the damage threshold $\kappa_0 = f_t/k_n$ in which $k_n$ is the normal stiffness of the joint. The history parameter $\kappa$ stores the largest value ever attained of the shifted equivalent displacement jump $[\![\mathrm{v}]\!]_{eq} = f([\![\mathrm{v}]\!])$, which is defined by a degenerated Drucker-Prager model, see [13].

### 3.2 Equilibrium path-following techniques

An important aspect in modelling masonry and other solids containing many nonlinearities is the use of a robust algorithm which is capable of tracing the whole equilibrium path, particularly the post-peak response of the structure. In this work, a modified arc-length constraint function is used to trace the equilibrium path of the shear wall and settlement tests (Sections 4.2 and 4.3). Since the nonlinear behaviour of the presented masonry model is solely governed by the enhanced degrees of freedom $\tilde{\mathbf{u}}$, they are used as the control variables in the path-following constraint function

$$g = \Delta\tilde{\mathbf{u}}^T \Delta\tilde{\mathbf{u}} - {\tau_{\mathrm{ARCL}}}^2 \tag{6}$$

in which $\tau_{\mathrm{ARCL}}$ represents the enforced arc-length of the equilibrium path during a load step. In the case of the simulation of a three-point bending test (Section 4.1), the crack mouth opening displacement (CMOD) of the lower middle joint is chosen as a control variable, similar to the experimental test setup [16]. The constraint function is then given by

$$g = s^T \Delta\mathbf{u} - \tau_{\mathrm{CMOD}} \tag{7}$$

where $s$ selects the enhanced degrees of freedom describing the crack opening of the considered joint, and $\tau_{\mathrm{CMOD}}$ denotes the allowed opening in one load step. Since at the start

of the calculation no enhanced degrees of freedom or CMOD are present, indirect displacement control, controlling the regular degrees of freedom, is used in the first load steps. The constraint function then becomes

$$g = s^T \Delta\hat{\mathbf{u}} - \tau_{\text{DISP}} \tag{8}$$

in which $s$ selects the degree of freedom where the displacement $\tau_{\text{DISP}}$ is enforced during the load step.

## 4 NUMERICAL EXAMPLES

### 4.1 Three-point bending test

In this first numerical example a three-point bending test is simulated. Brick arrangement and boundary conditions are reported in Figure 4. Material parameters (Tables 1 and 2) and experimental data (Figure 7) are obtained from [16]. Figure 5 depicts the active joints and deformed mesh at the final loading stage. The failure mode and corresponding load-CMOD diagram (Figure 7) shows a good correspondence with the experimental data and with the results from a model in which all joints are active at the start of the simulation (Figure 6). An indication of the computational efficiency is given by the evolution of the number of enhanced degrees of freedom during the computation, Figure 8.

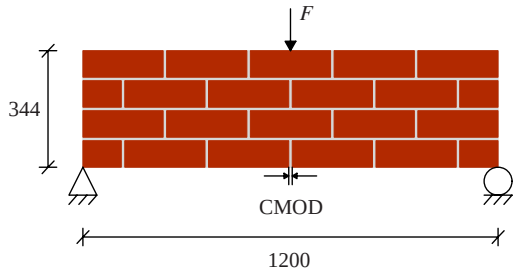


**Figure 4**: Test setup and boundary conditions for the three-point bending test. All dimensions are in mm.

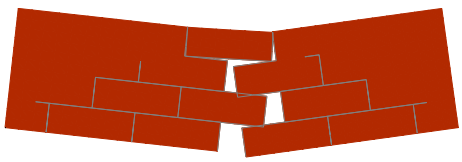

**Figure 5**: Deformed mesh and active joints (in grey) at a CMOD value of 2 mm. 40× displacement magnification.

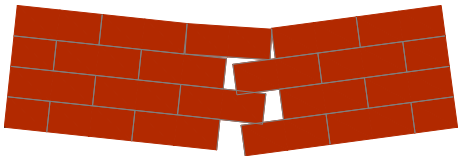

**Figure 6**: Deformed mesh at a CMOD value of 2 mm for a model with all joints a priori active. 40× displacement magnification.

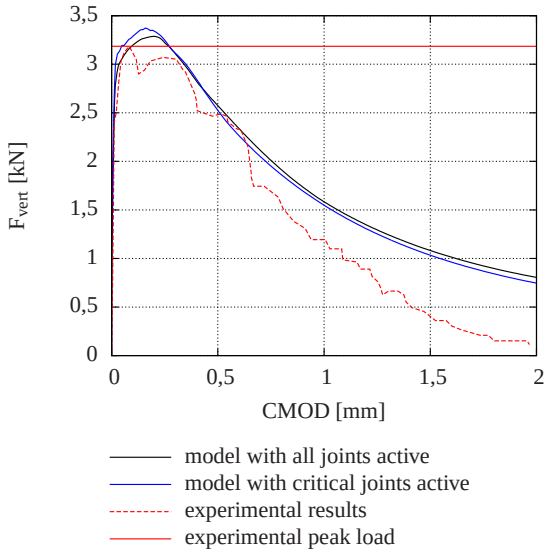


**Figure 7**: Simulation and experimental load-CMOD diagrams.

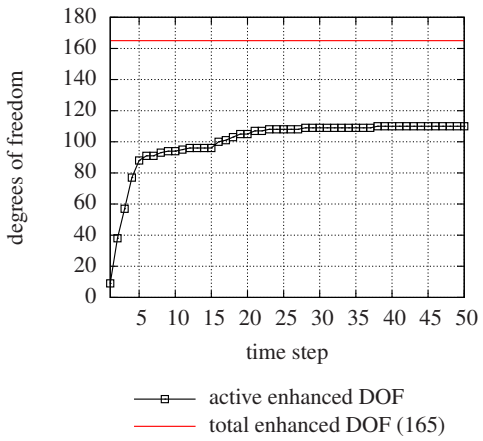


**Figure 8**: Evolution of the number of enhanced degrees of freedom.

**Table 1**: Setup and elastic material parameters for the three-point bending test.

| | dimensions | $E_b$ [N/mm$^2$] | $\nu$ | $k_n$ [N/mm$^3$] | $k_t$ [N/mm$^3$] | $\alpha$ |
|---|---|---|---|---|---|---|
| joints | 10 mm | | | 416 | 172 | |
| bricks | $76 \times 230 \times 110$ mm$^3$ | 17500 | 0,15 | | | 1,0 |

**Table 2**: Inelastic material parameters for the three-point bending test.

| | $f_t$ [N/mm$^2$] | $f_c$ [N/mm$^2$] | $f_b$ [N/mm$^2$] | $G_{f_I}$ [N/mm] |
|---|---|---|---|---|
| joints | 0,086 | 7,26 | 1,2 $f_c$ | 0,002 |

## 4.2 Shear wall test

The second example is a shear wall with opening [17]. Tables 3 and 4 list the material parameters. A confining stress of 0,30 N/mm$^2$ is applied on top of the wall prior to the application of the horizontal loading. Boundary conditions and test setup are depicted in Figure 9. Figures 10-13 show that both failure mode and peak load correspond with the experimental data and the results obtained with a masonry model in which all joints are a priori active. Figure 14 indicates that most of the computational gain of the presented algorithm is achieved during the first 30 load steps, i.e. the load steps prior to the peak load of the structure. After reaching the peak load, 80% of the enhanced degrees of freedom are activated.

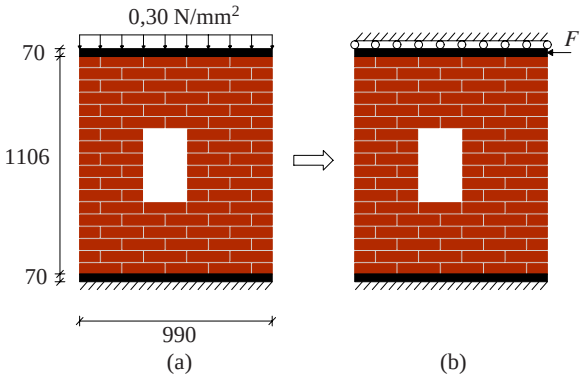


**Figure 9**: Test setup and boundary conditions for the shear wall test. (a) phase 1: confining load; (b) phase 2: horizontal loading. All dimensions are in mm.

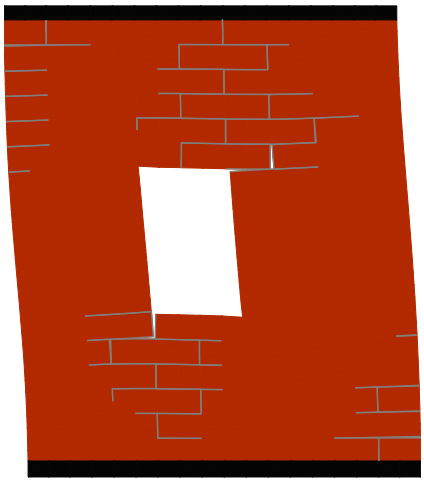

**Figure 10**: Deformed mesh and active joints (in grey) at a loading point displacement (LPD) of 0,5 mm. 100$\times$ displacement magnification.

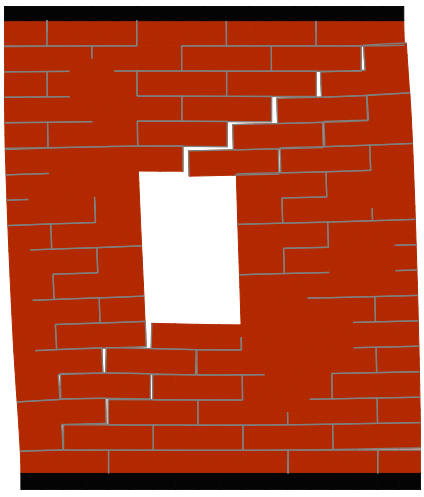

**Figure 11**: Deformed mesh and active joints (in grey) at a LPD value of 4 mm. 10$\times$ displacement magnification.

**Table 3**: Setup and elastic material parameters for the shear wall test.

| | dimensions | $E_b$ [N/mm$^2$] | $\nu$ | $k_n$ [N/mm$^3$] | $k_t$ [N/mm$^3$] | $\alpha$ |
|---|---|---|---|---|---|---|
| joints | 10 mm | | | 82 | 36 | |
| bricks | $52 \times 210 \times 100$ mm$^3$ | 16700 | 0,15 | | | 0,24 |

**Table 4**: Inelastic material parameters for the shear wall test.

| | $f_t$ [N/mm$^2$] | $f_c$ [N/mm$^2$] | $f_b$ [N/mm$^2$] | $G_{f_I}$ [N/mm] |
|---|---|---|---|---|
| joints | 0,25 | 10,5 | 1,2 $f_c$ | 0,018 |

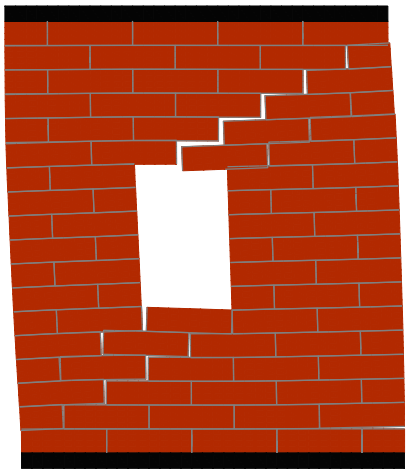

**Figure 12**: Deformed mesh at a LPD value of 4 mm for a model with all joints a priori active. 10× displacement magnification.

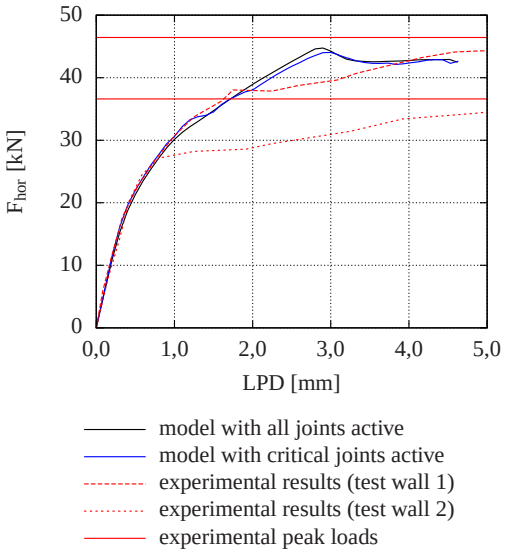


**Figure 13**: Simulation and experimental load-displacement diagrams.

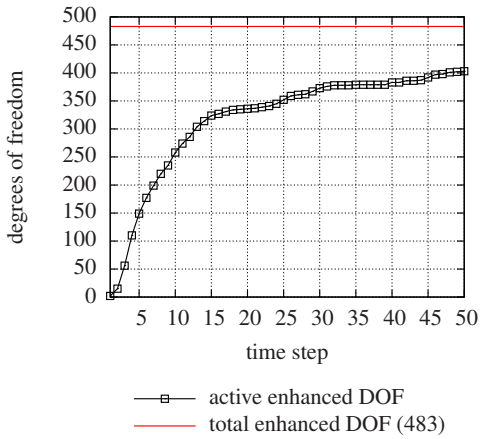


**Figure 14**: Evolution of the number of enhanced degrees of freedom.

### 4.3 Settlement test

As a final numerical example, an end-settlement of a blind wall is simulated. The material parameters are the same as for the shear wall test (Section 4.2), except the brick dimensions are 290 mm×190 mm×140 mm. The behaviour of the soil is governed by an interface element. Its normal compressive stiffness $k_{n,c} = 0{,}030$ N/mm$^2$ whereas the normal tensile stiffness and shear stiffness are zero. For $x < 0{,}6L$, the settlement $w$ takes the form [18]

$$w = \exp\left(-2\left(\frac{x - 0{,}6L}{0{,}4L - 0{,}6L}\right)^2\right) w_{end} \qquad (9)$$

in which $x$ is the distance from the left side of the wall, $L$ is the length of the system (5990 mm) and $w_{end}$ represents the settlement if $x \geq 0{,}6L$. Figures 15-16 depict the active

joints at an end-settlement of 6 mm and 12 mm, respectively. At the end of the loading process, nearly all joints are active indicating that the whole structure exhibits damage. However, the major damage localises in a typical staircase crack pattern, as observed in real structures subjected to severe settlements [19]. Finally, Figure 18 depicts the evolution of the amount of enhanced degrees of freedom during the computation.

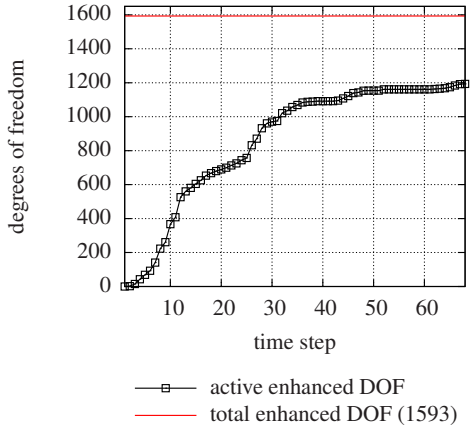


**Figure 18**: Evolution of the number of enhanced degrees of freedom.

## 5 CONCLUSIONS

In this contribution a new mesoscopic masonry model using the partition of unity method was presented. Joints are only explicitly modelled when a critical stress state is reached, resulting in a computationally more appealing procedure. In order to improve the robustness of the algorithm, a modified path-following technique is employed in which the enhanced degrees of freedom are taken as control variables in the arc-length constraint function. The performance of the new model is demonstrated by three-point bending, shear wall and settlement tests. Future work will include the use of more advanced material models that incorporate the initial orthotropic behaviour of the masonry. The partition of unity framework also allows straightforward applications such as the modelling of brick cracking and the modelling of irregular bond masonry using a simple mesh since the latter does not need to conform to the masonry joints.

## REFERENCES

[1] P. B. Lourenço, R. De Borst, and J. G. Rots. A plane stress softening plasticity model for orthotropic materials. *International Journal for Numerical Methods in Engineering*, 40(21):4033–4057, 1997.

[2] G. Milani. Simple homogenization model for the non-linear analysis of in-plane loaded masonry walls. *Computers & Structures*, 89(17-18):1586–1601, 2011.

[3] P. B. Lourenço and J. G. Rots. Multisurface interface model for analysis of masonry structures. *ASCE Journal of Engineering Mechanics*, 123(7):660–668, 1997.

[4] G. Giambanco, S. Rizzo, and R. Spallino. Numerical analysis of masonry structures via interface models. *Computer Methods in Applied Mechanics and Engineering*, 190(49-50):6493–6511, 2001.

[5] J. V. Alfaiate and J. R. de Almeida. Modelling discrete cracking on masonry walls. *Masonry International*, 17(2):83–93, 2004.

[6] G. Alfano and E. Sacco. Combining interface damage and friction in a cohesive-zone model. *International Journal for Numerical Methods in Engineering*, 68(5):542–582, 2006.

[7] K. De Proft, K. Heyens, and L. J. Sluys. Mesoscopic modelling of masonry failure. *Proceedings of the ICE - Engineering and Computational Mechanics*, 164(EM1):41–46, 2010.

[8] S. Brasile, R. Casciaro, and G. Formica. Multilevel approach for brick masonry walls - Part I: A numerical strategy for the nonlinear analysis. *Computer Methods in Applied Mechanics and Engineering*, 196(49-52):4934–4951, 2007.

[9] T. J. Massart, R. H. J. Peerlings, and M. G. D. Geers. An enhanced multi-scale

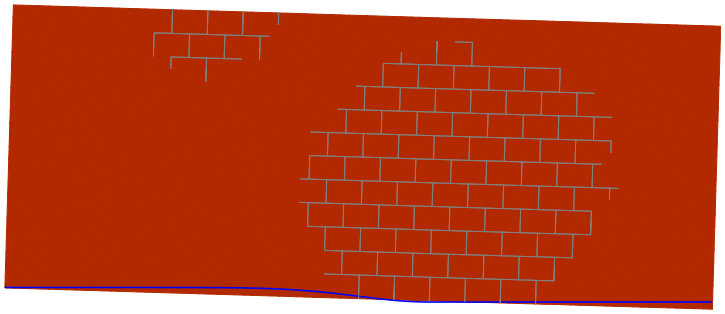

**Figure 15**: Deformed mesh and active joints (in grey) at end-settlement of 6 mm. 20× displacement magnification.

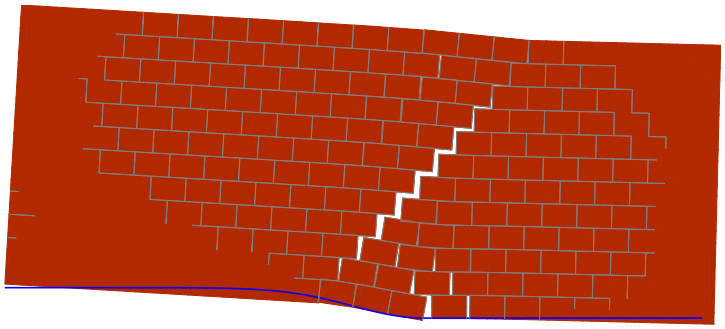

**Figure 16**: Deformed mesh and active joints (in grey) at end-settlement of 12 mm. 20× displacement magnification.

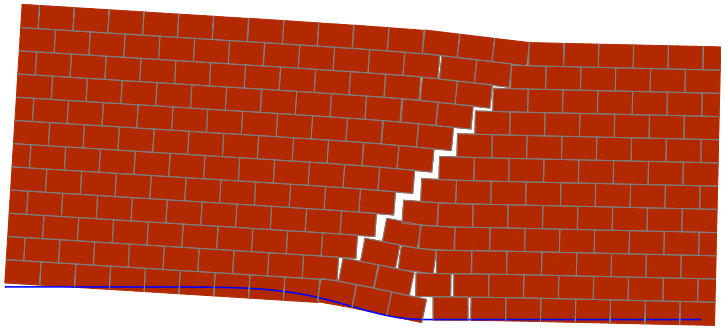

**Figure 17**: Deformed mesh at end-settlement of 12 mm for a model with all joints a priori active. 20× displacement magnification.

approach for masonry wall computations with localization of damage. *International Journal for Numerical Methods in Engineering*, 69(5):1022–1059, 2007.

[10] D. Addessi and E. Sacco. A multiscale enriched model for the analysis of masonry panels. *International Journal of Solids and Structures*, 49(6):865–880, 2012.

[11] S. Marfia and E. Sacco. Multiscale damage contact-friction model for periodic masonry walls. *Computer Methods in Applied Mechanics and Engineering*, 205-208:189–203, 2012.

[12] I. Babuska and J. M. Melenk. The partition of unity method. *International Journal for Numerical Methods in Engineering*, 40(4):727–758, 1997.

[13] B. Vandoren, K. De Proft, A. Simone, and L. J. Sluys. Mesoscopic modelling of masonry using weak and strong discontinuities. *Computer Methods in Applied Mechanics and Engineering*, in press (doi:10.1016/j.cma.2012.11.005).

[14] A. Simone, C. A. Duarte, and E. Van der Giessen. A Generalized Finite Element Method for polycrystals with discontinuous grain boundaries. *International Journal for Numerical Methods in Engineering*, 67(8):1122–1145, 2006.

[15] T. S. Hille, A. S. J. Suiker, and S. Turteltaub. Microcrack nucleation in thermal barrier coating systems. *Engineering Fracture Mechanics*, 76:813–825, 2009.

[16] K. Chaimoon and M. M. Attard. Experimental and numerical investigation of masonry under three-point bending (in-plane). *Engineering Structures*, 31(1):103–112, 2009.

[17] T. M. J. Raijkmakers and A. T. Vermeltvoort. Deformation controlled tests in masonry shear walls - Report B-92-1156. Technical report, TNO Bouw, 1992.

[18] R. B. Peck. Deep excavations and tunnelling in soft ground - state of the art report. In *Proceedings of the 7th International Conference on Soil Mechanics and Foundation Engineering, vol. 3*, pages 311–376, 1969.

[19] I. de Vent. *Structural damage in masonry. Developing diagnostic decision support*. PhD thesis, Delft University of Technology, 2011.